

Asymmetric Foucault pendulum dynamics with analogies to the Lipkin-Meshkov-Glick quantum phase transitions and other quantum phenomena

Tomáš Opatrný¹ and Pavel Štěpánek²

¹*Optics Department, Faculty of Science, Palacký University,
17. Listopadu 12, 77146 Olomouc, Czech Republic*

²*Mendel Gymnasium, Komenského 5, 746 01 Opava, Czech Republic*
(Dated: June 26, 2018)

Stokes parameter formalism is applied to show the analogies between the motion of an asymmetric Foucault pendulum and several phenomena known from optics and atomic physics. Nonlinearity-induced precession of elliptical orbits of the pendulum is shown to correspond to twisting transformations used for spin squeezing of atomic systems. Transitions between regimes of predominant nonlinearity and regimes where the Coriolis force or the asymmetry of the pendulum are dominant correspond to quantum phase transitions in the Lipkin-Meshkov-Glick model. A Foucault pendulum with highly anisotropic damping can emulate an optical Zeno effect where a sequence of polarizing filters inhibits polarization rotation of light in an optically active medium.

I. INTRODUCTION

To check whether Earth is still rotating, one can suspend a weight on a rope, start it swinging and observe the precession of its trajectory. The plane of swinging should precess with rate $\Omega_E \sin \lambda$, where Ω_E is the Earth's rotational angular velocity and λ is the geographic latitude. However, replicating the original Foucault's pendulum experiment of 1851 is not as easy as it sounds. Anybody who tried it for the first time has probably noticed a strange behavior: the horizontal projection of the trajectory changes from being a straight line to be approximately elliptical. Elliptical trajectories exhibit precession that is far from what one would naively expect considering just Earth's rotation. These problems have been studied since the days of the earliest experiments with Foucault's pendulums. In 1851 Airy showed that elliptical trajectories precess due to the nonlinear character of the spherical pendulum, the precession rate being proportional to the area of the ellipse [1] (for more recent derivations see [2–4]). Kamerlingh-Onnes in his dissertation of 1879 [5] studied a finely tuned Foucault's pendulum and showed that even a small asymmetry in the pendulum's construction leads to a transition from a straight trajectory to elliptical (for a discussion of Kamerlingh-Onnes' contribution in English see [6]). The primary observation was that the motion consists of perpendicular oscillations of different frequencies with the accumulated phase difference changing the trajectory shape.

A complete analytical description of the anisotropic spherical pendulum in a rotating system is rather involved and various aspects have been covered in extensive literature (see, e.g., [4, 7–9]). Here we present a simple intuitive picture that describes most of the important phenomena, based on the Stokes parameter formalism and the Poincaré sphere visualization. These tools are typically used to deal with the dynamics of polarized light or spin systems but seldom have been applied to mechanical motion (for a recent exception, see [10]). Surprisingly, the pendulum motion then can be mapped to various

phenomena that appear in completely different areas of physics. In particular, the Airy precession corresponds to the “one-axis-twisting” known from the physics of spin squeezing [11–16], whereas precession of the orbit due to the Coriolis force corresponds to the energy splitting, and the asymmetry-driven dynamics noted by Kamerlingh-Onnes to Rabi oscillations. Combining these effects, one finds behavior analogous to transitions between Josephson and Rabi regimes of trapped Bose-Einstein condensates or atomic spin systems [17–19], or more generally, to critical phenomena and quantum phase transitions in the Lipkin-Meshkov-Glick model [20–28]. When damping is included, other effects can occur; in particular, highly anisotropic damping can be used to simulate the “quantum Zeno effect” [29–31].

As stressed by Feynman in his lectures, “the same equations have the same solutions” [32] which makes it possible to transfer intuition between different areas of physics. Although, certainly, not all quantum effects can be emulated by a classical pendulum, we believe that our approach can offer a different and fresh perspective on well known phenomena. Thus, physicists from the atomic and optical community may be gratified to observe the same effects on their next visit to a science museum. Some of those effects can even get a rather simple interpretation. Such deep connections of the pendulum motion to other seemingly unrelated and distinct areas of physics could be also useful for those who build and study Foucault pendulums, when they encounter certain strange and unexpected dynamical behavior.

The paper is organized as follows. In Sec. II we introduce the Stokes parameters and their relation to the pendulum motion. In Sec. III conservative evolution equations are given and in Sec. IV their integrals of motion are studied and conditions for stationary points and their stability are determined. Section V deals with the damping. In Sec. VI we study the analogies of the system to other areas of physics. We summarize our main conclusions in Sec. VII.

II. ELLIPTICAL MOTION AND THE STOKES PARAMETERS

Let us assume that during a sufficiently short time interval the horizontal projection of the pendulum motion can be approximated by an ellipse with semi-axes a and b , and the major axis inclined at angle ψ to the x -axis, as shown in Fig. 1(a). The Cartesian variables are

$$x = a \cos \psi \cos \omega t - b \sin \psi \sin \omega t, \quad (1)$$

$$y = a \sin \psi \cos \omega t + b \cos \psi \sin \omega t. \quad (2)$$

The same ellipse can be described by amplitudes A and B in the directions x and y and their phase difference ϕ as

$$x = A \cos \omega t, \quad (3)$$

$$y = B \cos(\omega t - \phi), \quad (4)$$

ignoring an unimportant constant shift of the temporal origin in going from Eqs. (1)–(2) to Eqs. (3)–(4).

In analogy to describing a general elliptical polarization of light, we introduce (dimensionless) Stokes parameters as

$$S_0 \equiv \frac{2}{L^2} (\langle x^2 \rangle + \langle y^2 \rangle), \quad (5)$$

$$S_1 \equiv \frac{2}{L^2} (\langle x^2 \rangle - \langle y^2 \rangle), \quad (6)$$

$$S_2 \equiv \frac{4}{L^2} \langle xy \rangle, \quad (7)$$

$$S_3 \equiv \pm \frac{4}{L^2} \sqrt{\langle x^2 \rangle \langle y^2 \rangle - \langle xy \rangle^2}, \quad (8)$$

where L is the pendulum length. The average is over one period $T = 2\pi/\omega$, i.e., $\langle f(x, y) \rangle \equiv T^{-1} \int_0^T f(x, y) dt$, where $\omega = \sqrt{g/L}$ is the frequency of small oscillations of the pendulum and g is the acceleration due to gravity. The sign in Eq. (8) is positive (negative) for counter-clockwise (clockwise) motion, respectively. The Stokes parameters satisfy

$$S_0^2 = S_1^2 + S_2^2 + S_3^2, \quad (9)$$

and they can be used to visualize the polarization state as a point with coordinates (S_1, S_2, S_3) on a Poincaré sphere of radius S_0 , as in Fig. 1(b). Note that although working with a different approach, the recently introduced concept of “anisosphere” [10] describing motion of the Foucault pendulum is equivalent to the Poincaré sphere.

The Stokes parameters can be expressed in terms of the parameters of the ellipse as

$$S_0 = \frac{a^2 + b^2}{L^2}, \quad (10)$$

$$S_1 = \frac{a^2 - b^2}{L^2} \cos 2\psi, \quad (11)$$

$$S_2 = \frac{a^2 - b^2}{L^2} \sin 2\psi, \quad (12)$$

$$S_3 = \frac{2ab}{L^2}, \quad (13)$$

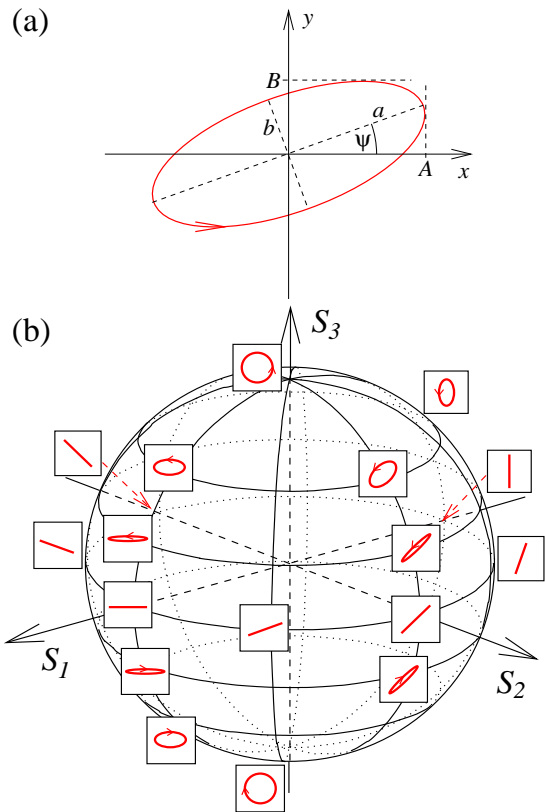


FIG. 1: (a) Scheme of the elliptical motion displaying the meaning of the parameters a , b , ψ , A and B . (b) Poincaré sphere with the corresponding trajectories of the pendulum. Circularly polarized trajectories occupy the poles, linearly polarized trajectories are localized on the equator and elliptical trajectories are on the rest of the surface.

or, alternately,

$$S_0 = \frac{A^2 + B^2}{L^2}, \quad (14)$$

$$S_1 = \frac{A^2 - B^2}{L^2}, \quad (15)$$

$$S_2 = \frac{2AB}{L^2} \cos \phi, \quad (16)$$

$$S_3 = \frac{2AB}{L^2} \sin \phi. \quad (17)$$

Parameters S_0 and S_3 have simple physical meanings: the energy of the pendulum is

$$E = \frac{1}{2} m \omega^2 L^2 S_0, \quad (18)$$

and the vertical component of its angular momentum is

$$\mathcal{L} = \frac{1}{2} m \omega L^2 S_3, \quad (19)$$

where m is the mass of the bob.

III. CONSERVATIVE TIME EVOLUTION

Let us first discuss three special kinds of evolution of the pendulum that will later be combined into unified motion.

A. Anisotropic oscillations

Assume that the frequency in x -direction is higher by $\Delta\omega$ than that in the y -direction, with $\Delta\omega \ll \omega$. This is typically caused by the directional dependence of elasticity in the suspension mechanism, or by asymmetric mass distribution in the physical pendulum as studied by Kamerlingh Onnes [5]. Then in Eqs. (3) and (4) the parameter ϕ varies with $\dot{\phi} = \Delta\omega$, whereas A and B are constant. Taking time derivatives of Eqs. (15)–(17) one finds

$$\dot{S}_1 = 0, \quad (20)$$

$$\dot{S}_2 = -\Delta\omega S_3, \quad (21)$$

$$\dot{S}_3 = \Delta\omega S_2, \quad (22)$$

which corresponds to the rotation of the Poincaré sphere around S_1 as in Fig. 2(a).

B. Motion in a rotating frame

Let us assume that the frame of reference rotates around z with angular velocity Ω , as in the case of Foucault pendulum. The Coriolis force then causes rotation of the pendulum orbit with angular velocity $-\Omega$, i.e., the inclination angle ψ of Eqs. (1) and (2) change at rate $\dot{\psi} = -\Omega$ while a and b remain constant. Taking time derivatives of Eqs. (11)–(13) one finds

$$\dot{S}_1 = 2\Omega S_2, \quad (23)$$

$$\dot{S}_2 = -2\Omega S_1, \quad (24)$$

$$\dot{S}_3 = 0, \quad (25)$$

which corresponds to the rotation of the Poincaré sphere around S_3 with *twice* the angular velocity of the coordinate system rotation (see Fig. 2(b)).

C. Precession due to pendulum nonlinearity

As first derived by Airy [1], the elliptical trajectory of a pendulum precesses with angular velocity $\tilde{\Omega}$ proportional to the area of the ellipse

$$\tilde{\Omega} = \frac{3ab}{8L^2}\omega, \quad (26)$$

the precession being in the same sense as the motion of the pendulum along the ellipse. This means that the

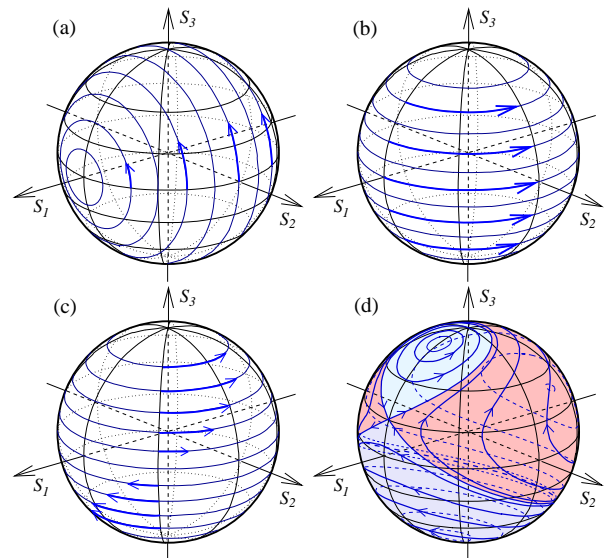


FIG. 2: Poincaré sphere trajectories for an asymmetric harmonic oscillator (a), symmetric harmonic oscillator in a rotating frame (b), spherical pendulum with Airy precession (c), and asymmetric pendulum in a rotating frame (d).

inclination angle ψ evolves as

$$\dot{\psi} = \tilde{\Omega} = \frac{3}{16}\omega S_3. \quad (27)$$

Using this in the time derivatives of Eqs. (11)–(13) yields

$$\dot{S}_1 = -\frac{3}{8}\omega S_2 S_3, \quad (28)$$

$$\dot{S}_2 = \frac{3}{8}\omega S_1 S_3, \quad (29)$$

$$\dot{S}_3 = 0. \quad (30)$$

This corresponds to *twisting* the Poincaré sphere: Individual points rotate around the S_3 -axis, their angular velocity being proportional to the value of S_3 . The corresponding motion is shown in Fig. 2(c).

D. Combined motion

Combining all the three effects, the resulting equations of motion are

$$\begin{aligned} \dot{S}_1 &= 2\Omega S_2 - \frac{3}{8}\omega S_2 S_3, \\ \dot{S}_2 &= -2\Omega S_1 - \Delta\omega S_3 + \frac{3}{8}\omega S_1 S_3, \\ \dot{S}_3 &= \Delta\omega S_2. \end{aligned} \quad (31)$$

This is a nonlinear set of equations that can be solved numerically, an example of which is shown in Fig. 2(d). However, one can find integrals of motion from which trajectories can be expressed analytically.

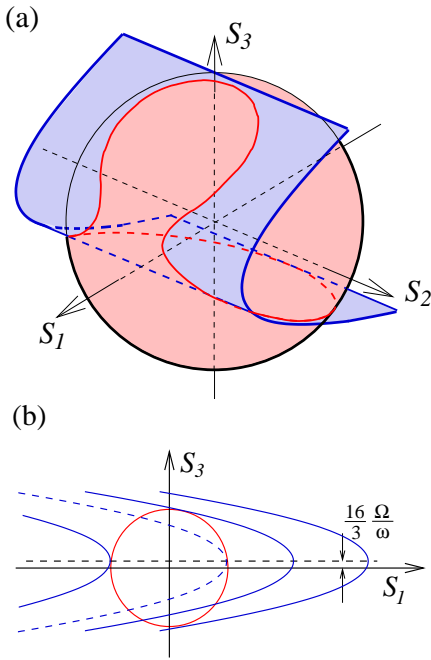


FIG. 3: (a) Poincaré sphere trajectory as an intersection of the sphere $S_0 = \text{const}$ and a parabolic cone $H = \text{const}$. (b) Stationary points as points of touch of the sphere and parabolic cones. The full lines represent the cones touching at the stable stationary points, the broken line represents the cone touching at the unstable stationary point.

IV. INTEGRALS OF MOTION, TRAJECTORIES AND STATIONARY POINTS

There are two integrals of motion related to the set (31), namely S_0^2 of Eq. (9) and H given by

$$H = \Delta\omega S_1 - 2\Omega S_3 + \frac{3}{16}\omega S_3^2. \quad (32)$$

This can be checked by taking time derivatives dS_0^2/dt of Eq. (9) and dH/dt of Eq. (32) and applying there Eqs. (31). Therefore, trajectories in the (S_1, S_2, S_3) coordinates are lines of intersection of a sphere $S_0^2 = \text{const}$ and a parabolic cylinder $H = \text{const}$ (see Fig. 3(a)).

The trajectories reduce to stationary points where the sphere barely touches the parabolic cylinder (see Fig. 3(b)). They can be found from Eq. (31) by setting the left-hand side equal to zero. Thus for $\Delta\omega \neq 0$ one finds $S_2 = 0$ and by expressing S_3 and inserting it into equation $S_1^2 + S_3^2 = S_0^2$ one gets

$$S_1^4 - \frac{8\Delta\omega}{3\omega} S_1^3 + \left[\left(\frac{4\Omega}{3\omega} \right)^2 + \left(\frac{4\Delta\omega}{3\omega} \right)^2 - S_0^2 \right] S_1^2 + \frac{8\Delta\omega}{3\omega} S_0^2 S_1 - \left(\frac{4\Delta\omega}{3\omega} \right)^2 S_0^2 = 0. \quad (33)$$

Eq. (33) has up to 4 real roots for S_1 in the interval between $-S_0$ and S_0 .

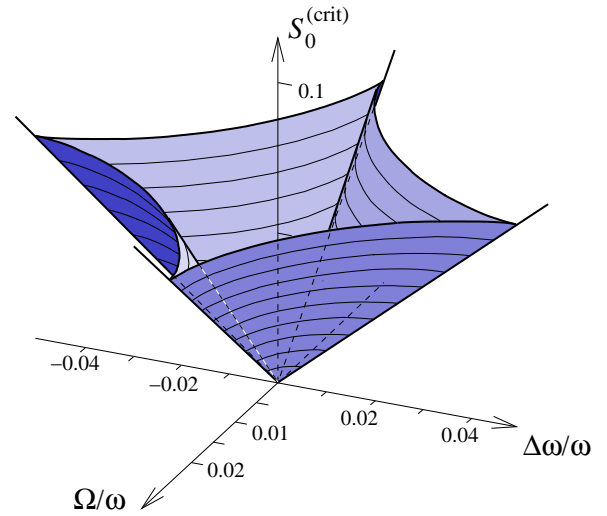


FIG. 4: Dependence of the critical value $S_0^{(\text{crit})}$ on $\Delta\omega$ and Ω as in Eq. (34). Inside the surface the nonlinearity is dominant and unstable stationary points exist; outside the linear terms are dominant and the equations of motion have just two stable stationary points.

In the special case of a symmetric pendulum, $\Delta\omega = 0$, the parabolic cylinder reduces to a pair of planes perpendicular to S_3 . Two stable stationary points are the poles of the Poincaré sphere $S_1 = S_2 = 0$, $S_3 = \pm S_0$ corresponding to circular polarizations. In case of $S_0 > 16|\Omega|/(3\omega)$ there is a circle of unstable stationary points with $S_3 = 16\Omega/(3\omega)$.

Another special case corresponds to an asymmetric pendulum with no rotation, $\Omega = 0$. Here the parabolic cylinder has a plane of symmetry $S_1 = 0$ and two of the stationary points are $S_1 = \pm S_0$, $S_2 = S_3 = 0$. If $S_0 > 8|\Delta\omega|/(3\omega)$, then the radius of the sphere is bigger than one of the principal radii of the cylinder at the point of their contact. In this case, the point where the cylinder touches the sphere from inside is unstable. This can be seen by observing nearby trajectories that occur if the cylinder is shifted by a slight change of H : locally the trajectories are hyperbolas rather than ellipses as would be the case of a stable stationary point. Apart from the stable and unstable points at $S_1 = \pm S_0$, two additional stable stationary points occur at $S_1 = 8\Delta\omega/(3\omega)$, $S_2 = 0$, $S_3 = \pm\sqrt{S_0^2 - S_1^2}$.

In the general case of four stationary points, three of them are stable and one is unstable. Again, the unstable stationary point corresponds to the parabolic cylinder touching the sphere from inside at a point where one of the principal radii of the cylinder is smaller than the radius of the sphere. From a simple geometric consideration we find the critical value of the radius

$$S_0^{(\text{crit})} = \frac{8}{3} \frac{[\Delta\omega^{2/3} + (2\Omega)^{2/3}]^{3/2}}{\omega} \quad (34)$$

above which such kind of contact can occur (see A for the derivation). This function is shown in Fig. 4. Thus, for

$S_0 > S_0^{(\text{crit})}$ there are three stable and one unstable stationary points. For $S_0 = S_0^{(\text{crit})}$ two stable points merge with the unstable point forming one stable point, and for $S_0 < S_0^{(\text{crit})}$ only two stable points exist.

In the case of two stationary points all trajectories encircle the stationary points in the same sense. In the case of four stationary points the Poincaré sphere is divided into three separate areas, each containing one stationary point encircled by the trajectories. These areas shown in different colors in Fig. 2(d) are separated by a line called *separatrix* that crosses itself at the unstable stationary point.

In terms of the pendulum motion, consider first a non-rotating system with $\Omega = 0$, $\Delta\omega \neq 0$, and $S_0 > S_0^{(\text{crit})}$. Two of the stationary points correspond to elliptical polarizations with the larger axis along the fast direction of the pendulum, the pendulum orbiting in opposite sense in the two cases. The third stationary point corresponds to the linear polarization along the slow direction of the pendulum. Linear polarization along the fast direction of the pendulum is unstable; if the pendulum is swung in this direction, the motion would soon change into elliptical and evolve depending on the exact value of the initial condition. In rotating systems with $\Omega \neq 0$ the stationary points move towards the north or south pole, depending on the sign of Ω . Each of the stationary points now corresponds to some general elliptical polarization.

V. DAMPED MOTION

Various kinds of damping can be included in the model to modify the equations of motion. Here we study a particularly simple situation of linear, in general anisotropic damping. Assume a damping force $\vec{F} \equiv (F_x, F_y) = -(c_x \dot{x}, c_y \dot{y})$ where $c_{x,y} \geq 0$ are constants. The special case of $c_x = c_y$ corresponds, e.g., to viscous damping of the pendulum bob due to air drag with low Reynolds numbers. The anisotropic case of $c_x \neq c_y$ could stem, e.g., from viscous damping in a Cardan suspension of the pendulum. Using these forces in the equations of weakly damped harmonic oscillators one finds the time change of the amplitudes as

$$\dot{A} = -\frac{\gamma_x}{2}A, \quad (35)$$

$$\dot{B} = -\frac{\gamma_y}{2}B, \quad (36)$$

where $\gamma_{x,y} = c_{x,y}/m$, which leads to

$$\dot{S}_0 = -\frac{\gamma_x + \gamma_y}{2}S_0 - \frac{\gamma_x - \gamma_y}{2}S_1, \quad (37)$$

$$\dot{S}_1 = -\frac{\gamma_x - \gamma_y}{2}S_0 - \frac{\gamma_x + \gamma_y}{2}S_1, \quad (38)$$

$$\dot{S}_2 = -\frac{\gamma_x + \gamma_y}{2}S_2, \quad (39)$$

$$\dot{S}_3 = -\frac{\gamma_x + \gamma_y}{2}S_3. \quad (40)$$

Note that in Eq. (38) S_0 can be expressed as $S_0 = \sqrt{S_1^2 + S_2^2 + S_3^2}$ so that three equations (although nonlinear) for $S_{1,2,3}$ are enough to govern the Stokes vector motion.

In the isotropic case of $\gamma_x = \gamma_y \equiv \gamma$, all the Stokes parameters are damped with the same rate, $\dot{S}_k = -\gamma S_k$, for $k = 0, \dots, 3$. Another extreme case is the unidirectional damping with $\gamma_x \equiv \gamma$, $\gamma_y = 0$, where we get

$$\dot{S}_0 = -\frac{\gamma}{2}S_0 - \frac{\gamma}{2}S_1, \quad (41)$$

$$\dot{S}_1 = -\frac{\gamma}{2}S_0 - \frac{\gamma}{2}S_1, \quad (42)$$

$$\dot{S}_2 = -\frac{\gamma}{2}S_2, \quad (43)$$

$$\dot{S}_3 = -\frac{\gamma}{2}S_3. \quad (44)$$

In this case the maximum dissipation rate occurs for $S_{2,3} = 0$, $S_1 = S_0$, where $\dot{S}_{0,1} = -\gamma S_{0,1}$, whereas no dissipation takes place for $S_{2,3} = 0$, $S_1 = -S_0$, where $\dot{S}_{0,1} = 0$.

In a similar way one can also treat more general forms of damping, although the equations become more involved and will be studied elsewhere.

VI. RELATION TO OTHER AREAS OF PHYSICS

A. Polarized light and Zeno effect

The poles of the Poincaré sphere correspond to circularly polarized light whereas the points on the equator represent different linearly polarized states. Rotation around the vertical axis as in Fig. 2(b) corresponds to rotation of the polarization plane by optically active media such as a sugar solution. Rotation around a horizontal axis as in Fig. 2(a) is caused by anisotropic media in which vertically polarized light propagates with different speed from horizontally polarized light. Devices made of such materials are used, for example, to convert circularly polarized light into linear (a quarter-wave plate) such as in some glasses used for 3D cinema.

Anisotropic damping corresponds to dichroism, i.e., to light absorption depending on the linear polarization. A polarization filter can be modeled by extremely anisotropic damping, e.g., a pendulum with a Cardan suspension with vanishing friction in one direction and substantial friction in the perpendicular direction: after a certain time, only the oscillations in the undamped direction survive.

An optical ‘‘Zeno effect’’ [29] can be observed when a sequence of polarizers is inserted into the optically active medium [30, 31]. Assume first a slab of optically active medium of such a width that the linear polarization of a passing light beam rotates by $\pi/2$. If two filters of the same polarization direction are added, one at the input and the other at the output of the slab,

then no light can go through. Insert now a sequence of equidistant filters into the medium, their polarization directions being the same as that of the input and output filters. Since each of the filters projects the beam polarization to that of the input filter, some light can now pass through. In the limit of infinitely many perfect filters the system becomes perfectly transparent for the light that passes through the first filter. This is a seeming paradox, since adding absorbing elements actually decreases the resulting absorption. In quantum physics the effect corresponds to measurements that project a system to the input state. Frequent measurements then lead to the inhibition of evolution of the system: One can “stop the motion by watching”.

An analogous effect can be observed with a Foucault pendulum and highly anisotropic damping. With no damping, the plane of swinging would rotate by $\pi/2$ in time $T_{\pi/2} = \pi/(2\Omega)$. With anisotropic damping $0 \approx \gamma_y < \Omega \ll \gamma_x$, and with the pendulum initially swinging in the undamped direction y , it will stay swinging in the same direction with almost no losses. If, on the other hand, the damping is switched on only at the beginning and after time $T_{\pi/2}$ (equivalent to only the input and output filters present), then all the pendulum’s energy will be absorbed by the damping mechanism.

B. Spin systems and Bose-Einstein condensates

Eq. (32) can be written in an operator form to define a quantum Hamiltonian

$$\hat{H} = \Delta\omega\hat{S}_1 - 2\Omega\hat{S}_3 + \frac{3}{16}\omega\hat{S}_3^2, \quad (45)$$

with $\hat{S}_{1,2,3}$ commuting as $[\hat{S}_k, \hat{S}_l] = i\epsilon_{jkl}\hat{S}_j$, where ϵ_{jkl} is the Levi-Civita symbol, and Einstein summation convention is used. Operators $\hat{S}_{1,2,3}$ can be used to describe the collective spin of N spin-half particles, with $\hat{S}_0^2 \equiv \hat{S}_1^2 + \hat{S}_2^2 + \hat{S}_3^2$ being a constant related to the particle number as $\hat{S}_0^2 = \frac{N}{2}(\frac{N}{2} + 1)$. The evolution can be expressed in the form of Heisenberg equations $d\hat{S}_k/dt = i[\hat{H}, \hat{S}_k]$ with $\hbar = 1$. The resulting equations of motion correspond to Eq. (31) with operator products being symmetrized as $S_k S_l \rightarrow \frac{1}{2}(\hat{S}_k \hat{S}_l + \hat{S}_l \hat{S}_k)$.

Points on the Poincaré sphere (in spin physics commonly called the Bloch sphere) correspond to spin-polarized states along the corresponding directions. Thus, for example, the north pole corresponds to all spins up whereas the south pole to all spins down. The dynamics described in Sec. III corresponds to several well-known effects of spin physics. If the spin-up and spin-down states have different energies then the sphere rotates around S_3 as in Fig. 2(b) at a rate proportional to the energy difference. To rotate the sphere around a horizontal axis as in Fig. 2(a), a resonant microwave field can be applied. The spin then exhibits Rabi oscillations. The rotation rate is proportional to the intensity of the

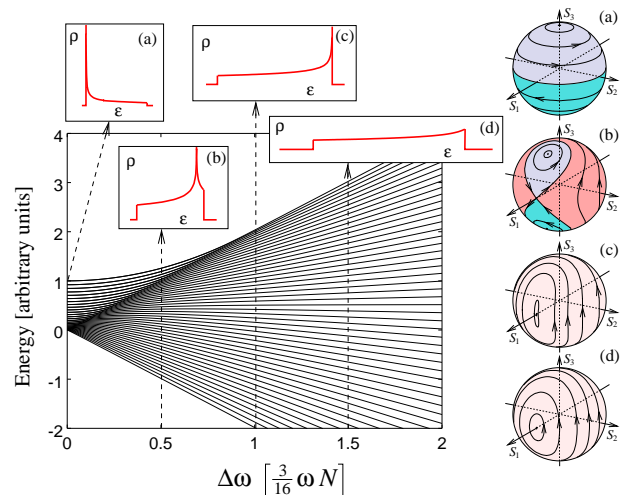


FIG. 5: Dependence of eigenvalues of the Hamiltonian (45) on $\Delta\omega$ for $N = 50$ and $\Omega = 0$. The insets show the spectral densities $\rho(\epsilon)$ in the limit of $N \rightarrow \infty$, i.e., the relative numbers of eigenstates in rescaled energy intervals $d\epsilon$ for $\Delta\omega = 0$ (a), $\Delta\omega = 0.5 \cdot \frac{3}{16}\omega N$ (b), $\Delta\omega = \frac{3}{16}\omega N$ (c), and $\Delta\omega = 1.5 \cdot \frac{3}{16}\omega N$ (d). The Poincaré spheres on the right show the corresponding classical pendulum trajectories with substituting S_0 for $N/2$. The regime of dominant nonlinearity is in the range of $\Delta\omega$ between cases (a) and (c) and is characterized by a diverging peak of the density of states that travels from the bottom of the energy spectrum (a) to the top (c). In the pendulum motion this corresponds to the existence of unstable stationary points. In case (a) the whole equator is formed from unstable stationary points, in the regime between (a) and (c), with a particular example of case (b) a single unstable point exists. Case (c) corresponds to the critical value of $\Delta\omega$ where the unstable point merges with two stable points resulting in a stable stationary point. For higher $\Delta\omega$, as in the example (d), the density of states is smooth and there are only two stationary points in the pendulum motion that are stable.

field and the orientation of the rotational axis depends on the phase of the field.

The twisting operation as in Fig. 2(c) is achieved in collective spin systems with mutual interactions. The corresponding operation is used to generate *spin squeezing*, as first proposed by Kitagawa and Ueda [11] and experimentally demonstrated in [12–15]. To understand it, consider a collection of N spins initially prepared each in the same superposition $2^{-1/2}(|\uparrow\rangle + |\downarrow\rangle)$. The collective state can be visualized, on the Bloch sphere of radius $N/2$, as a circle with its center at the equator and diameter (characterizing the uncertainty of spin projections) $\sim \sqrt{N}$. The twisting operation governed by Hamiltonian $\hat{H} \propto \hat{S}_3^2$ then deforms the circle, stretching it in one direction and squeezing in the perpendicular one. As a result, one obtains a collective spin state with decreased (“squeezed”) noise of some observable quantity. This quantity then can be used for enhanced precision measurements. Various combinations of the linear terms together with the quadratic one in Hamiltonian (32) can

be used to optimize the squeezing procedure. In this way, the dynamics of Fig. 2(d) corresponds to a variant of the “twist-and-turn” scenario for spin squeezing [16, 33]. Imagine a state located at the unstable stationary point of Fig. 2(d). Its uncertainty circle is very efficiently stretched and squeezed in the directions of the arrows along the separatrix.

The same formalism can be used to describe dynamics of a Bose-Einstein condensate (BEC) located in a double-well trap [17] or in a ring trap with grating [27]. Rather than two spin orientations, the atoms can have two different localizations of the double-well or two orbital states in the ring. Tunneling of atoms between the wells corresponds to the rotation of the sphere around a horizontal axis, and mutual repulsion (or attraction) of the atoms leads to the twisting operation. Circling around one of the stable stationary points near a pole corresponds to an effect called “self-trapping” of the BEC in a “Josephson regime” [18]: even though a single atom would tunnel back and forth between the two wells, the atomic interaction can keep a BEC in a single well. An analogous effect can be seen in an asymmetric pendulum: in linear regime, if initialized with a circular orbit, the pendulum would exhibit “Rabi flips”, switching between clockwise and counterclockwise orientations of the orbit. In the nonlinear regime (sufficiently high amplitude) the pendulum can be “self-trapped” in one of these orbital orientations.

C. “Spin squeezing” with a classical pendulum

Consider an ensemble of identical pendulums, each initialized near the x -oriented linearly polarized state. To be more specific, in the initial ensemble, the mean values of the Stokes parameters are $\bar{S}_1 \approx S_0$, $\bar{S}_2 = 0$ and $\bar{S}_3 = 0$, and the standard deviations are $\Delta S_2 = \Delta S_3 \equiv \Delta \ll S_0$, with no correlation between S_2 and S_3 . After being left to evolve, the elliptical states with positive S_3 move by the Airy precession in the opposite direction compared to states with negative S_3 . As a result, S_2 and S_3 become correlated and the ensemble forms a stretched area on the Poincaré sphere. After a sufficiently long time τ with $8/(3\omega S_0) \ll \tau \lesssim 4/(3\omega\Delta)$ the ensemble area has approximate dimensions $\Delta_+ \approx (3/8)S_0\omega\tau\Delta$ and $\Delta_- \approx 8\Delta/(3S_0\omega\tau)$ and is tilted by angle $\alpha \approx 8/(3S_0\omega\tau)$ from the equator. When $\Delta_- < \Delta$ the ensemble is “squeezed”. To remove the correlation and see the “squeezing” directly as in the spin-squeezing experiments, one can temporarily switch on the pendulum anisotropy to rotate the sphere around S_1 by angle α so as to align the stretched area with the equator. The ensemble is now squeezed in S_3 , meaning that the elliptical component is suppressed and all the states are now closer to the linear polarization than at the beginning. The price is the increased uncertainty in the orientation of the linear polarization corresponding to the ensemble being stretched along the equator.

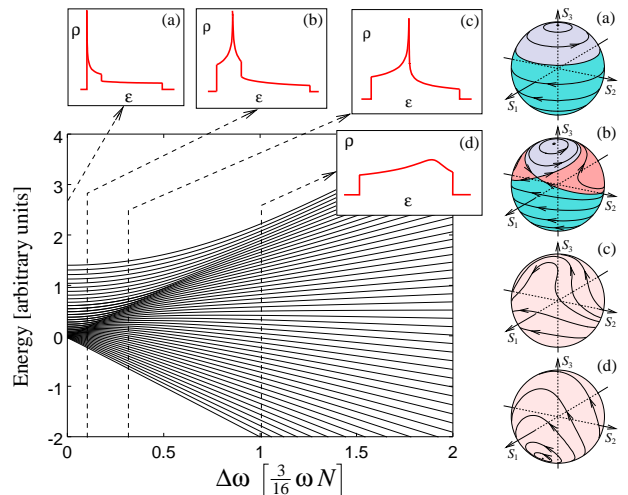


FIG. 6: Same as Fig. 5, but with $\Omega = 0.2 \cdot \frac{3}{16} \omega N$. The insets and the Poincaré spheres correspond to $\Delta\omega = 0$ (a), $\Delta\omega = 0.1 \cdot \frac{3}{16} \omega N$ (b), $\Delta\omega = 0.309 \cdot \frac{3}{16} \omega N$ (c), and $\Delta\omega = \frac{3}{16} \omega N$ (d). Case (c) corresponds to the critical value of $\Delta\omega$ where the unstable stationary point merges with one of the stable points. Differently from Fig. 5, in the nonlinear regime the density of states has a discontinuity (apart from the diverging peak) that corresponds to a local maximum of the Hamiltonian. For the critical value of $\Delta\omega$ the diverging peak merges with the discontinuity, forming a smooth maximum of ρ for higher values of $\Delta\omega$.

Note that squeezing with classical Hamiltonians has been explored in [34] with the focus on finding a general formula for the squeezing rate.

D. Lipkin-Meshkov-Glick model and quantum phase transitions

In 1965 Lipkin, Meshkov and Glick (LMG) formulated a toy model of multiparticle interaction that can be, under certain conditions, solved exactly, and thus serve as a basis for testing various approximation methods [20]. Although the original motivation was modeling energy spectra of atomic nuclei, the scheme turned out to be useful for studying critical phenomena in much more general systems. It has been shown that in the LMG model ground-state, quantum phase transition can occur [21], a concept later generalized to excited-state quantum phase transitions [22]. Since then, phase transitions in the LMG model have been studied in great detail (see, e.g., [23–27]). Recently the LMG phase transitions have been shown to correspond to transitions between regimes of classical motion of rigid bodies with rotors [28].

The LMG Hamiltonian has the form

$$\hat{H}_{\text{LMG}} = \epsilon \hat{S}_3 + V(\hat{S}_1^2 - \hat{S}_2^2) + W(\hat{S}_1^2 + \hat{S}_2^2), \quad (46)$$

where ϵ, V and W are real parameters. In the special case of $V = 0$ the LMG Hamiltonian is equivalent to

$$\hat{H} = \epsilon \hat{S}_3 - W \hat{S}_3^2, \quad (47)$$

where we have subtracted a constant term $W(\hat{S}_1^2 + \hat{S}_2^2 + \hat{S}_3^2) = W\frac{N}{2}(\frac{N}{2} + 1)$ that does not influence the dynamics. Compared with Eq. (32), we can see that the model corresponds to a symmetric Foucault pendulum with $W = -(3/16)\omega$ and $\epsilon = -2\Omega$. For large N , the Hamiltonian (47) is known to transit through a critical point at $S_0 = |\epsilon/W|$ (following, for example, the considerations of [24, 25]): For lower values the linear term dominates and the energy spectrum is smooth. For higher values of S_0 the nonlinearity dominates and a discontinuity in the energy spectrum occurs: the change is called a *quantum phase transition*. The situation corresponds to the occurrence of a circle of unstable stationary points on the Poincaré sphere for $S_0 > 16\Omega/(3\omega)$, which follows from Eq. (34) if we set $\Delta\omega = 0$.

Another special case is $V = -W$. Relabeling the variables $\hat{S}_1 \rightarrow \hat{S}_2 \rightarrow \hat{S}_3 \rightarrow \hat{S}_1$ then leads to the Hamiltonian

$$\hat{H} = \epsilon\hat{S}_1 + 2W\hat{S}_3^2 \quad (48)$$

that corresponds to an asymmetric pendulum with $\Omega = 0$, $\epsilon = \Delta\omega$ and $2W = (3/16)\omega$. Also here a quantum phase transition occurs, now at $S_0 = |\epsilon/(4W)|$. For lower S_0 the linear term is dominant and the spectrum is smooth; for higher values of S_0 a discontinuity in the spectrum occurs corresponding to the occurrence of the unstable stationary point on the Poincaré sphere for $S_0 > 8\Delta\omega/(3\omega)$. Experimental observation of such a bifurcation in collective atomic spins has been reported in [19]. We illustrate the correspondence of the quantum and classical models in Fig. 5.

The general case of both $\Delta\omega \neq 0$ and $\Omega \neq 0$ is not included in the original LMG Hamiltonian (46), but can be treated as a generalized LMG model (see, e.g., [23, 28]). In Fig. 6 we show the transition through the critical point with keeping Ω constant and varying $\Delta\omega$. The effect can be observed in interacting spin systems by applying suitable resonant and off-resonant electromagnetic fields, or in a Foucault pendulum on rotating Earth by varying the asymmetry in the elasticity of the suspension.

Note that when comparing the quantum and classical critical phenomena, S_0 was always considered small in the classical model, whereas in the quantum systems the corresponding parameter $N/2$ goes to infinity in the thermodynamic limit. This is the consequence of our choice of the length scale. It is convenient to compare the amplitude of the oscillations with the pendulum length L ; therefore in the definition of S_k in Eqs. (5)–(8) there is L^2 in the denominator and $S_k < 1$. If, instead, the length unit were chosen as the size of the vacuum fluctuations $(\hbar/2m\omega)^{1/2}$, then the magnitudes of the dimensionless parameters S_0 and $N/2$ would match.

VII. CONCLUSION

We have discussed a straightforward analogy between the motion of Foucault-type pendulums and the dynamics of various optical and quantum mechanical physical

systems. Our approach is based on reducing the dimensionality of the spherical pendulum problem. Out of the complete 4D phase space of the system we give up one variable: by averaging out the phase, the remaining dynamical variables can be chosen as the three independent Stokes coordinates $S_{1,2,3}$. There are two integrals of motion which can be visualized as a sphere and a parabolic cylinder, their lines of intersection determining the trajectories. The geometric interpretation allows us to identify the boundary between regimes of dominant nonlinearity with unstable stationary points, and linearity-dominated regimes with just two stable stationary points. As we checked numerically, the evolution of the reduced model very truly reproduces behavior of the full pendulum model in the regime of $\Omega, \Delta\omega \ll \omega$ and reasonably small amplitudes, $S_0 \lesssim 0.3$. Deviations from the exact evolution of the pendulum stem from the difference between the actual shape of the orbit and its approximation as an ellipse.

The classical evolution equations correspond to the quantum mechanical Heisenberg equations of the LMG model with relevance to BEC dynamics or spin squeezing. Even though many interesting quantum phenomena have their counterparts in the pendulum dynamics, there are essential differences as well. Whereas the classical set of equations (31) is closed, the operator equations generated by the quantum Hamiltonian (45) do not lead to a closed set of equations for their moments: one gets an infinite chain of equations, each coupling to higher order moments. As a result, a quantum system can develop features that are beyond the classical description. Interference structures of Schrödinger cat-like states is one of possible examples. Having in mind the essential differences, our results can be useful in transferring intuition between rather different areas of physics.

Appendix A: Proof of Eq. (34)

From Eq. (32) express S_1 as a function of S_3 and find the radius of the curvature of the parabola as $R = (1 + S_1'^2)^{3/2}/|S_1''|$, where $S_1' = dS_1/dS_3$. We get

$$R = \frac{8|\Delta\omega|}{3\omega} \left[1 + \left(\frac{2\Omega}{\Delta\omega} - \frac{3\omega}{8\Delta\omega} S_3 \right)^2 \right]^{3/2}. \quad (A1)$$

For a point on a circle with radius R centered at the line $S_3 = 0$ we find the relation between the coordinate S_3 and the derivative S_1' as

$$S_3 = \pm R \frac{S_1'}{\sqrt{1 + S_1'^2}}. \quad (A2)$$

Putting equal the radii of the parabola and the circle at a point where the derivatives S_1' of both curves are equal we find

$$S_3 = \frac{8\Delta\omega}{3\omega} \left[\frac{2\Omega}{\Delta\omega} + \left(\frac{2\Omega}{\Delta\omega} \right)^{1/3} \right], \quad (A3)$$

which inserted into Eq. (A1) leads to Eq. (34) for $S_0 = R$.

Acknowledgment

T.O. is grateful to K. K. Das for stimulating discussions. This work was supported by the Czech Science

Foundation, grant No. 17-20479S.

-
- [1] G. B. Airy, *On the Vibration of a Free Pendulum in an Oval Differing little from a Straight Line*. *Memoirs of the Royal Astronomical Society* **20**, 121–130 (1851).
- [2] M. G. Olsson, *The precessing spherical pendulum*. *Am. J. Phys.* **46**, 1118–1119 (1978).
- [3] M. G. Olsson, *Spherical pendulum revisited*. *Am. J. Phys.* **49**, 531–534 (1981).
- [4] H. R. Maya, R. A. Diaz, and W. J. Herrera, *Study of the apsidal precession of the Physical Symmetrical Pendulum*. *Journal of Applied Mechanics* **82**, 021008 (2015). arXiv:1312.4019
- [5] H. Kamerlingh Onnes, *Nieuwe Bewijzen voor de aswenteling der aarde*. Ph.D. thesis, University of Groningen, NL, 1879. Available through Niedersächsische Staats- und Universitätsbibliothek Digitalisierungszentrum, Goettingen.
- [6] E. O. Schulz-DuBois, *Foucault Pendulum Experiment by Kamerlingh Onnes and Degenerate Perturbation Theory*. *Am. J. Phys.* **18**, 173–188 (1970).
- [7] K. F. Johansen and T. R. Kane, *A simple description of the motion of a spherical Pendulum*. *J. Appl. Mech.* **36**, 76–82. (1969)
- [8] D. D. Holm, *Geometric Mechanics - Part I: Dynamics and Symmetry*. Imperial College Press; 2 edition (2011).
- [9] R. Moeckel, *The Foucault Pendulum (with a Twist)*. *SIAM Review* **59**, 369–389 (2017).
- [10] R. Verreault, *The anisosphere as a new tool for interpreting Foucault pendulum experiments. Part I: harmonic oscillators*. *Eur. Phys. J. Appl. Phys.* **79**, 31001 (2017).
- [11] M. Kitagawa and M. Ueda, *Squeezed spin states*. *Phys. Rev. A* **47**, 5138 (1993).
- [12] J. Esteve, C. Gross, A. Weller, S. Giovanazzi, and M. K. Oberthaler, *Squeezing and entanglement in a Bose-Einstein condensate*. *Nature* **455**, 1216 (2008).
- [13] C. Gross, T. Zibold, E. Nicklas, J. Esteve, and M. K. Oberthaler, *Nonlinear atom interferometer surpasses classical precision limit*. *Nature* **464**, 1165 (2010).
- [14] M. F. Riedel, P. Böhi, Y. Li, T. W. Hänsch, A. Sinatra, and P. Treutlein, *Atom-chip-based generation of entanglement for quantum metrology*. *Nature* **464**, 1170 (2010).
- [15] I. D. Leroux, M. H. Schleier-Smith, and V. Vuletić, *Implementation of Cavity Squeezing of a Collective Atomic Spin*. *Phys. Rev. Lett.* **104**, 073602 (2010).
- [16] T. Opatrný, *Twisting tensor and spin squeezing*. *Phys. Rev. A* **91**, 053826 (2015).
- [17] A. Smerzi, S. Fantoni, S. Giovanazzi, and S. R. Shenoy, *Quantum coherent atomic tunneling between two trapped Bose-Einstein condensates*. *Phys. Rev. Lett.* **79**, 4950 (1997).
- [18] A. J. Leggett, *Bose-Einstein condensation in the alkali gases: Some fundamental concepts*. *Rev. Mod. Phys.* **73**, 307 (2001).
- [19] T. Zibold, E. Nicklas, C. Gross, and M. K. Oberthaler, *Classical Bifurcation at the Transition from Rabi to Josephson Dynamics*. *Phys. Rev. Lett.* **105**, 204101 (2010).
- [20] H. J. Lipkin, N. Meshkov, A.J. Glick, *Validity of many-body approximation methods for a solvable model: (I). Exact solutions and perturbation theory*. *Nuclear Physics* **62**, 188 (1965).
- [21] Gilmore, R. & Feng, D. H. Phase transitions in nuclear matter described by pseudospin Hamiltonians. *Nucl. Phys. A* **301**, 189–204 (1978).
- [22] Cejnar, P., Macek, M., Heinze, S., Jolie, J. & Dobe, J. Monodromy and excited-state quantum phase transitions in integrable systems: collective vibrations of nuclei. *J. Phys. A: Math. Gen.* **39**, L515 (2006).
- [23] J. Vidal, *Concurrence in collective models*. *Phys. Rev. A* **73**, 062318 (2006).
- [24] O. Castaños et al, *Classical and quantum phase transitions in the Lipkin-Meshkov-Glick model*. *Phys. Rev. B* **74**, 104118 (2006).
- [25] P. Ribeiro, J. Vidal, and R. Mosseri, *Thermodynamical Limit of the Lipkin-Meshkov-Glick Model*. *Phys. Rev. Lett.* **99**, 050402 (2007).
- [26] M.A. Caprio, P. Cejnar, and F. Iachello, *Excited state quantum phase transitions in many-body systems*. *Annals of Physics* **323**, 1106 (2008).
- [27] T. Opatrný, M. Kolář and K. K. Das, *Spin squeezing by tensor twisting and Lipkin-Meshkov-Glick dynamics in a toroidal Bose-Einstein condensate with spatially modulated nonlinearity*. *Phys. Rev. A* **91**, 053612 (2015).
- [28] T. Opatrný, L. Richterek, and M. Opatrný, *Analogies of the classical Euler top with a rotor to spin squeezing and quantum phase transitions in a generalized Lipkin-Meshkov-Glick model*. *Sci. Rep.* **8**, 1984 (2018).
- [29] B. Misra and E. C. G. Sudarshan, *The Zeno's paradox in quantum theory*. *J. Math. Phys.* **18**, 756 (1977).
- [30] A. Peres, *Zeno paradox in quantum theory*. *Am. J. Phys.* **48**, 931 (1980).
- [31] I. Gonzalo, M. A. Porrás, and A. Luis, *Zeno inhibition of polarization rotation in an optically active medium*. *Eur. J. Phys.* **36**, 045001 (2015).
- [32] R. P. Feynman, R. B. Leighton, and M. Sands, *The Feynman Lectures on Physics*. (Addison Wesley Longman 1970) Volume II Chap. 121.
- [33] W. Muessel, H. Strobel, D. Linnemann, T. Zibold, B. Juliá-Díaz, and M. K. Oberthaler, *Twist-and-turn spin squeezing in Bose-Einstein condensates*. *Phys. Rev. A* **92**, 023603 (2015).
- [34] T. Opatrný, *Squeezing with classical Hamiltonians*. *Phys. Rev. A* **92**, 033801 (2015).